Functional Versatility of a Series of Zr MOFs Probed by Solid-State Photoluminescence Spectroscopy

Journal:	*Journal of the American Chemical Society*
Manuscript ID	ja-2017-02184x.R1
Manuscript Type:	Article
Date Submitted by the Author:	n/a
Complete List of Authors:	Marshall, Ross; University of Glasgow, Kalinovskyy, Yaroslav; University of Kent, School of Physical Science Griffin, Sarah; University of Glasgow, Wilson, Claire; University of Glasgow, Blight, Barry; University of Kent, School of Physical Science Forgan, Ross; University of Glasgow, School of Chemistry

Functional Versatility of a Series of Zr MOFs Probed by Solid-State Photoluminescence Spectroscopy

Ross J. Marshall,[a] Yaroslav Kalinovskyy,[b] Sarah L. Griffin,[a] Claire Wilson,[a] Barry A. Blight[b,c]* and Ross S. Forgan[a]*

[a]*WestCHEM, School of Chemistry, University of Glasgow, University Avenue, Glasgow, G12 8QQ, UK.*

[b]*School of Physical Sciences, University of Kent, Ingram Building, Canterbury, CT2 7NH, UK.*

[c]*Department of Chemistry, University of New Brunswick, Toole Hall, Fredericton, NB, E3B 5A3, Canada.*

ABSTRACT: Many of the desirable properties of metal-organic frameworks (MOFs) can be tuned by chemical functionalization of the organic ligands that connect their metal clusters into multidimensional network solids. When these linker molecules are intrinsically fluorescent, they can pass on this property to the resultant MOF, potentially generating solid-state sensors, as analytes can be bound within their porous interiors. Herein, we report the synthesis of a series of 14 interpenetrated Zr and Hf MOFs linked by functionalized 4,4′-[1,4-phenylene-bis(ethyne-2,1-diyl)]-dibenzoate (peb^{2-}) ligands, and analyse the effect of functional group incorporation on their structures and properties. Addition of methyl, fluoro, naphthyl and benzothiadiazolyl units does not affect the underlying topology, but induces subtle structural changes, such as ligand rotation, and mediates host-guest interactions. Further, we demonstrate that solid-state photoluminescence spectroscopy can be used to probe these effects. For instance, introduction of naphthyl and benzothiadiazolyl units yields MOFs that can act as stable fluorescent water sensors, a dimethyl modified MOF exhibits a temperature dependent phase change controlled by steric clashes between interpenetrated nets, and a tetrafluorinated analogue is found to be superhydrophobic despite only partial fluorination of its organic backbone. These subtle changes in ligand structure coupled with the consistent framework topology give rise to a series of MOFs with a remarkable range of physical properties that are not observed with the ligands alone.

Introduction

Metal-organic frameworks (MOFs)[1-7] are multidimensional network materials containing both inorganic and organic constituents. The diverse choice of organic and inorganic units that can be used to construct MOFs results in a wide variety of structures.[8-10] The high porosity of MOFs has prompted investigations towards potential applications such as gas capture and storage,[11-16] catalysis,[5,17-19] sensing[20-22] and drug delivery.[23-26] Lately, many synthetic efforts towards MOFs have focused on those containing group IV transition metal ions, especially zirconium and hafnium.[27-32] Zr and Hf MOFs linked by linear dicarboxylate ligands generally adopt the well-documented UiO-66 topology (UiO = University of Oslo) which contains $M_6O_4(OH)_4$ clusters (M = Zr or Hf) linked in three dimensions by twelve bridging organic ligands.[27] Alternative topologies of Zr and Hf MOFs have been obtained, usually with non-linear carboxylate ligands,[33-37] whilst extended organic ligands have resulted in interpenetrated UiO-66 analogues.[38,39] Members of this series of Zr MOFs are constructed from substituted 4,4′-[1,4-phenylene-bis(ethyne-2,1-diyl)]-dibenzoate (peb^{2-}) ligands (Figure 1a) and exhibit a two-fold interpenetrated structure (Figure 1b).[38]

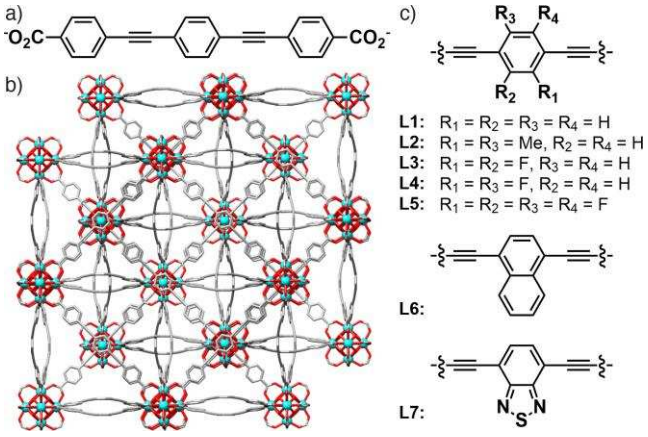

Figure 1. a) Chemical structure of 4,4′-[1,4-phenylene-bis(ethyne-2,1-diyl)]-dibenzoate, peb^{2-}, termed **L1** herein, alongside b) the solid-state packing structure of the interpenetrated MOF it forms with Zr, termed **Zr-L1**. c) Structural description and naming scheme of the functionalized peb^{2-} ligands used throughout this study.

This family of Zr MOFs has been extended to include an anthracene derivative[40] and functionalized analogues designed for postsynthetic modification (PSM), while they have been investigated for catalytic applications[40-42] and also CO_2 separation.[43] We are particularly interested in Zr

MOFs containing integral alkyne moieties,[44] having recently demonstrated their successful postsynthetic halogenation for potential use as I_2 sequestration materials,[45] and for their ability to modulate the mechanical properties of Zr MOFs, which can be manipulated by the choice of organic ligand.[46,47]

In 2005, a report detailing the optical properties of the dimethyl ester of the π-conjugated peb^{2-} ligand (**L1-Me$_2$**), demonstrated that this ligand precursor exhibited strong absorption in the UV region and was strongly fluorescent, with a quantum yield of 0.91 (λ_{abs} = 335 nm) in dichloromethane.[48] Since then, the Zr MOF containing peb^{2-} (**Zr-L1**; Figure 1b) has been investigated for photocatalytic organic dye degradation; optical measurements and DFT calculations confirmed that the optical properties of the MOF are inherited from the π-conjugated organic ligand.[41] A number of other fluorescent zirconium MOFs have been reported and many of them have been used for the detection and sensing of analytes such as metals,[49] explosives,[50] harmful gases/vapours[51-53] and antibiotics.[54] Alternatively, the intrinsic fluorescence of Zr MOFs has been demonstrated to be useful in pH sensing,[55,56] while changes in ligand conformation in tetraphenylethylene-[57] and porphyrin-linked[58] Zr MOFs has been shown to result in differences in their steady state emission spectra, both in terms of band positions and intensities.

Inspired by the intrinsic fluorescence of **L1-Me$_2$**, we herein report the synthesis and structural/optical characterization of a series of interpenetrated Zr and Hf MOFs containing substituted peb^{2-} ligands. We have varied the chemical substituents on the central core of the extended ligand to include methyl, fluorine, naphthyl and benzothiadiazolyl moieties (Figure 1c). We detail how linker functionalization modulates the structural and optical properties of the resulting Zr and Hf MOFs, whose unusual structural features and host-guest behavior have been probed *via* solid-state emission techniques.

Results and Discussion

The dimethyl esters of each of the ligands shown in Figure 1c (see SI, Scheme S1) were synthesized by Pd/Cu catalysed Sonogashira cross-coupling reactions, followed by saponification to produce the free acids (see SI, Section S2). Solvothermal reactions containing the required ligand, $ZrCl_4$ or $HfCl_4$, hydrochloric acid, and either benzoic acid[59] or L-proline[60,61] as modulators in DMF resulted in the isolation of a series of new interpenetrated Zr and Hf MOFs (see SI, Section S3). Careful choice of reaction parameters, such as concentration, temperature and modulator choice/equivalency resulted in the isolation of fourteen highly crystalline interpenetrated Zr and Hf MOFs. We described the solid-state structures of $[M_6O_4(OH)_4(\mathbf{L1})_6]_n$ (M = Zr or Hf) recently[45] (Figure 1b) and this repeating formula is common to all fourteen MOFs. The MOFs are herein described as **M-Ln**, where **M** is either Zr or Hf and **Ln** is the ligand used to construct the framework.

Powder X-ray diffraction (PXRD) was used to first analyse the bulk phase purity of the MOFs that were isolated from the synthetic mixtures by centrifugation. Initial attempts at bulk MOF syntheses were performed using our recently discovered L-proline modulation,[60] which proved again to be very efficient. L-proline effectively modulated twelve of the fourteen MOFs, however it did not produce Zr or Hf MOFs containing the tetrafluoro ligand (**L5**), which is unexpected considering the di-fluorinated ligands (**L3** and **L4**) were compatible with these synthetic conditions. Instead, we turned to benzoic acid modulation[59] for **Zr-L5** and **Hf-L5** and bulk microcrystalline samples were successfully obtained. Upon comparison of the PXRD patterns of the Zr MOFs, it is immediately obvious that all the MOFs are highly crystalline and structurally very similar (Figure 2a), while the Hf MOFs display analogous structures (see SI, Section S4).

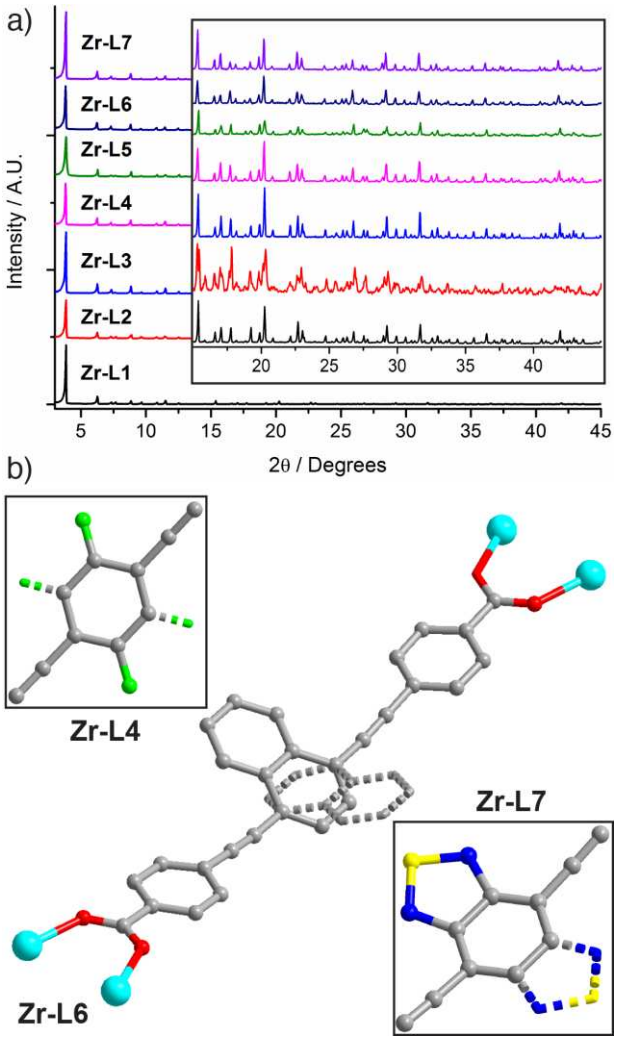

Figure 2. a) Comparison of the PXRD patterns of the Zr MOFs synthesized during this study, with the inset highlighting the high angle data. The analogous data for the Hf MOFs are provided in the SI, Section S4. b) Portions of the solid-state structures of **Zr-L4**, which shows positional disorder of the fluorine atoms on the ligand core; **Zr-L6**, highlighting the two disordered arrangements of the naphthyl moieties which rotate out of the plane of conjugation; and **Zr-L7**, showing disorder of the thiadiazolyl units over both sides of the ligand.

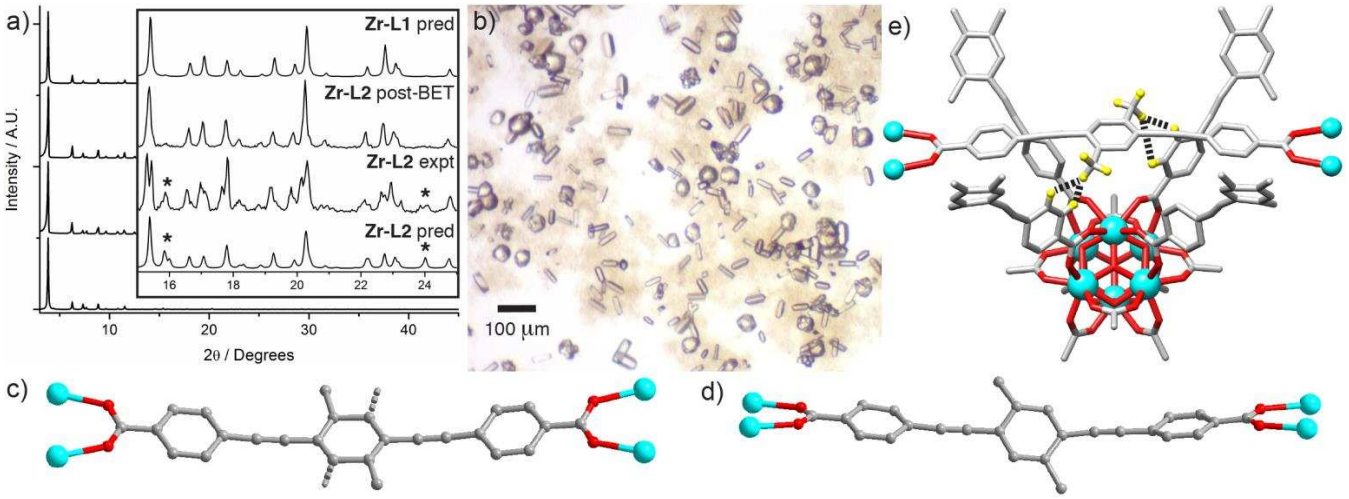

Figure 3. a) PXRD patterns of **Zr-L2** before and after N_2 adsorption measurements compared with predicted patterns of MOFs with orthorhombic and cubic symmetry. Peaks marked with an asterisk are lost on activation, indicating a phase change. b) Optical microscope image of single crystals of **Zr-L2**. c) and d) represent the planar and twisted orientations of **L2** observed within **Zr-L2**, respectively. e) A portion of the solid-state structure of **Zr-L2** (protons and disordered methyl groups have been omitted for clarity) with dashed lines representing the close proximity of the pendant methyl groups with the other framework.

Optimization of reaction conditions resulted in the isolation of single crystals of thirteen of the MOFs, with **Hf-L2** being the only MOF that could not be prepared as diffraction quality single crystals. The crystal structures of the Zr and Hf analogues of individual ligands are very similar, as expected based on the close structural agreement between **Zr-L1** and **Hf-L1**.[45] The pendant functionality of the ligands does not disrupt formation of the MOFs with all materials displaying two-fold interpenetration. Crystal structures of the Zr and Hf MOFs containing the di-fluorinated ligands **L3** and **L4** display positional disorder of the fluorine atoms across all four sites of the central phenylene ring and, on first inspection they, all appear to be identical and resemble the MOFs containing **L5**. The positional disorder, however, is accounted for by adjusting chemical occupancies (Figure 2b). Similarly, the benzothiadiazolyl unit of **L7** is disordered across two orientations in **Zr-L7** and **Hf-L7**, maintaining the cubic symmetry despite the lower symmetry of the ligand. Interestingly, we observe differences in the solid-state structures of **Hf-L6** and **Zr-L6**, which contain naphthyl units. In **Hf-L6** there is similar positional disorder of the naphthyl unit across both sides of the ligand, while in **Zr-L6** the same disorder is observed, however in this case the naphthyl core twists out of the plane of conjugation of the ligand by approximately 23°, presumably to minimise steric interactions with other linkers in the interpenetrated structure. The reason for the different behaviour in the Zr and Hf analogues has not been established.

All the functionalized MOFs discussed thus far adopt the typical cubic structure and crystallise with the *Fd-3m* symmetry of the parent MOFs, however, close inspection of the PXRD patterns reveals slight differences observed for MOFs containing **L2** (Figure 3a), with additional peaks observed. Single crystals of **Zr-L2** (Figure 3b) have both lozenge-shaped and rounded morphologies, unlike the typical well-defined octahedral crystals of the other members of the series.

Both of these forms of **Zr-L2** crystallize in the lower symmetry orthorhombic *Imma* space group, but have the same connectivity and composition of the other MOFs, and this is attributed to the presence of different ligand orientations. Of the twelve ligands connected to each Zr_6 cluster, four ligands in an equatorial plane are planar with disordered methyl units (Figure 3c) while the other eight ligands adopt a conformation where the central dimethylphenylene unit is twisted by approximately 40° out of the plane of conjugation, and the methyl groups are fully ordered (Figure 3d). Twisting of the ligands in **Zr-L2** is believed to be the result of steric interactions between the bulky methyl groups and adjacent phenyl units of the other interpenetrated net, which are in close proximity (Figure 3e).

It is interesting to note that **L4**, which contains fluorine atoms in same positions that **L2** contains methyl groups, can be incorporated into Zr and Hf MOFs with the expected cubic symmetry, as the steric interactions imposed by the fluorine atoms are insufficient to drive the structural perturbation observed in **Zr-L2**. In the crystal structure of **Zr-L2** the ligands of one net bow away from the Zr_6 cluster of the second net, while in **Zr-L4** and the rest of the MOFs the ligands bow in towards the cluster, and this structural difference is likely to be due to the differing extent of steric interactions (see SI, Section S5).

The PXRD pattern of **Zr-L2** changed significantly over the course of N_2 adsorption experiments (Figure 3a). Comparing the experimental PXRD pattern of chloroform exchanged **Zr-L2** (**Zr-L2** expt) with the predicted pattern from the orthorhombic single crystal structure (**Zr-L2** pred), it is clear that some of the peaks match well, while some of them are split, indicating the presence of multiple phases.

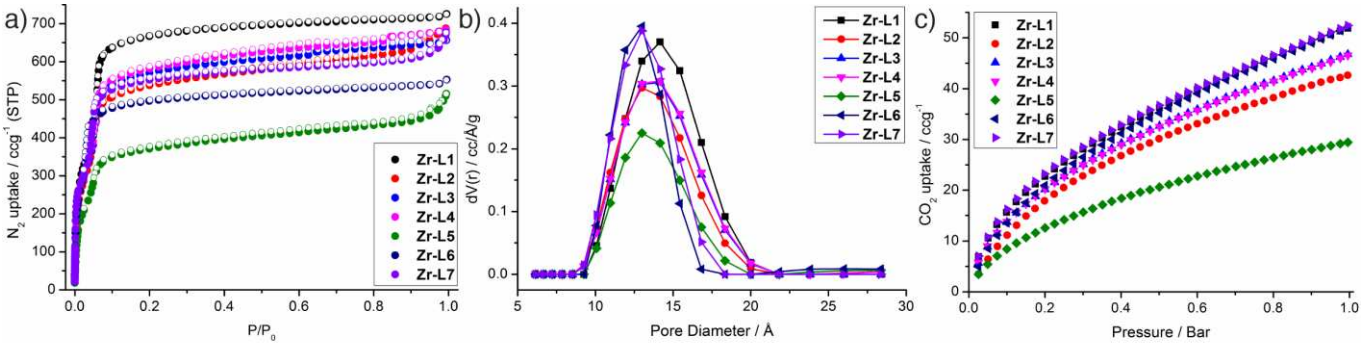

d)

	L1	L2	L3	L4	L5	L6	L7
Zr	2680 m^2g^{-1}	2070 m^2g^{-1}	2195 m^2g^{-1}	2270 m^2g^{-1}	1420 m^2g^{-1}	1990 m^2g^{-1}	2130 m^2g^{-1}
Hf	2080 m^2g^{-1}	1775 m^2g^{-1}	1800 m^2g^{-1}	1960 m^2g^{-1}	675 m^2g^{-1}	1210 m^2g^{-1}	1660 m^2g^{-1}

Figure 4. a) N_2 adsorption and desorption isotherms collected at 77 K for the Zr MOFs. b) Corresponding pore size distributions (QSDFT) for the MOF series. Analogous data for the Hf MOFs are given in the SI, Section S7. c) CO_2 adsorption isotherms (273 K) of the Zr MOFs. d) Calculated BET surface areas for all fourteen Zr and Hf MOFs.

The PXRD pattern of cubic **Zr-L1** was also predicted (**Zr-L1** pred), revealing that the experimental pattern of chloroform exchanged **Zr-L2** resembles both the orthorhombic and cubic predicted patterns to some extent, again suggesting a mixture of two phases. The presence of mixed phases of **Zr-L2** suggests that the material is dynamic and that it may be able to transition from the orthorhombic (*Imma*) to the cubic (*Fd-3m*) phase by rotation of the central dimethylphenylene units. This is indeed confirmed by PXRD analysis of **Zr-L2** after N_2 adsorption experiments (**Zr-L2** post-BET) with the pattern now in excellent agreement with the predicted pattern for cubic **Zr-L1**. Prior to N_2 uptake experiments the material was activated by heating at 120 °C for 20 hours and we believe that, upon heating, the ligands rotate to adopt the linear geometry found in the cubic MOFs. We further investigated this phenomenon by performing variable temperature PXRD and the same trend is observed, confirming that heating results in a structural modification and crystallographic phase change (see SI, Section S5).

With the series of interpenetrated Zr and Hf MOFs in hand, we decided to analyse and compare the effect of substitution on their physical properties. From the thermogravimetric analysis (TGA) profiles (see SI, Section S6) it is clear that the thermal stabilities of the materials are relatively unaffected by the presence of either Zr_6 or Hf_6 clusters with degradation occurring at approximately the same temperature. TGA experiments were performed under an air atmosphere, resulting in decomposition of the MOFs to either ZrO_2 or HfO_2, and the increased mass of Hf relative to Zr accounts for the smaller percentage mass losses that are observed for the Hf MOFs. Ligand functionalization results in slightly altered thermal properties, however there is no obvious negative impact on the MOFs' thermal stabilities, with all fourteen materials decomposing at ~450–500 °C.

Comparing the N_2 uptakes of the Zr MOFs (see SI, Section S7 and Figure 4a) it is evident that ligand functionalization results in a reduction in gravimetric N_2 uptake compared with **Zr-L1,** as would be expected. The N_2 uptakes of **Zr-L2**, **Zr-L3** and **Zr-L4** are similar, which is reassuring as all three MOFs contain two pendant moieties of similar mass: either methyl groups or fluorine atoms. The porosity of **Zr-L7** is similar to that of the MOFs containing pendant di-methyl/fluorine moieties, whilst **Zr-L6** displays a slightly lower uptake. The reason for the lower than expected BET surface area of **Zr-L5** (1420 m^2g^{-1}) is not immediately obvious, however, low values were consistently observed for multiple batches. It should be noted that the uptake of **Hf-L5** (675 m^2g^{-1}) is also lower than expected, and therefore it may be plausible that the activation conditions were ineffective for MOFs containing **L5** or that during activation the MOFs were partially collapsing. The calculated pore-size distributions (QSDFT) are consistent with the functional groups occupying the pore space of the MOFs, with an observed reduction of the main pore diameter from 14.2 Å in **Zr-L1** to 13.0 Å in **Zr-L7** (Figure 4b). Similar trends were observed for the Hf MOFs. CO_2 uptake isotherms of the Zr MOFs were collected at 0 °C (see SI, Section S7) to examine the potential for MOF-guest interactions and reveal that while ligand functionalization does not significantly improve the CO_2 uptake capacities under the pressure range investigated (Figure 4c), the similar uptakes obtained for **Zr-L1**, **Zr-L6** and **Zr-L7** (they are superimposed in Figure 4c) suggest that naphthyl and benzothiadiazolyl units do enhance CO_2 uptake to some extent. This enhancement comes in spite of the incorporation of bulky aromatics/heterocycles, presumably through favourable interactions between CO_2 and either the π-system of **Zr-L6** or the electron rich heterocycle of **Zr-L7**, which has been observed previously in a related Cu-MOF.[62]

Given that **L1-Me$_2$** and its derivatives exhibit interesting absorption properties, and with the incorporation of known chromophores such as naphthyl[63,64] and benzothiadiazolyl[65,66] units into the MOFs, solid-state UV-Vis (SS-UV-Vis) spectra of all the **Zr-Ln** MOFs were collected (Figure 5a) and compared with those of the dimethyl es-

ters (the diesters are a better model for the Zr MOFs as hydrogen bonding between carboxylates is nullified) and free acids of the ligands (see SI, Section S8). The comparisons revealed that in most cases the spectroscopic properties of the MOFs are generally inherited from the respective ligand.

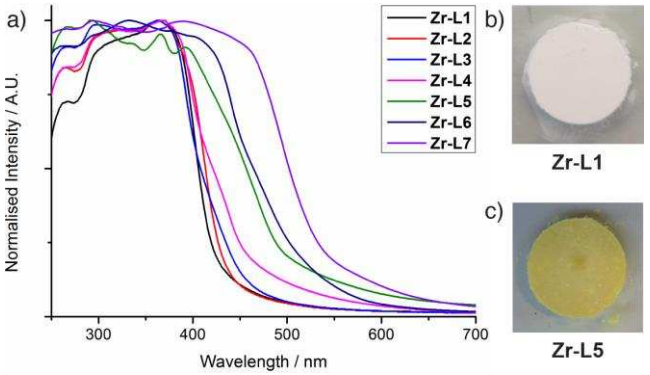

Figure 5. a) Comparison of the solid-state UV-Vis spectra of the Zr MOFs. Photographs of b) **Zr-L1** and c) **Zr-L5** highlight the unexpected intense yellow colour of **Zr-L5**.

In particular, it is clear that the benzothiadiazolyl containing MOF (**Zr-L7**; a deep yellow solid) absorbs furthest into the visible region (~600 nm), with its strongest absorbance occurring at λ_{max} = 391 nm. **Zr-L6**, a pale yellow solid comprised of naphthyl chromophores, also absorbs well into the visible region (λ_{max} = 333 nm), aligning well with the absorption properties of **L6-Me$_2$**. Similarly, **Zr-L5** absorbs in the visible region and is yellow (Figure 5c), correlating well with the SS-UV-Vis spectra, despite **L5-H$_2$** and **L5-Me$_2$** being white. The red-shifted absorption of **Zr-L5** relative to that of **L5-Me$_2$** can be ascribed to an LMCT transition that appears as a shoulder at approximately 460 nm.[67] These transitions have been well described for both Zr^{IV} and Ti^{IV} based UiO-66 systems,[68] and here are further redshifted due to the high degree of conjugation within these peb^{2-} ligand systems. More generally, the transitions would be more appropriately described as ligand-to-cluster charge transfer (LCCT) since any participation in the CT comes from a cumulative cluster-centred energy state.[69]

The SS-UV-Vis absorption features of the MOFs and the conjugated nature of their bridging ligands prompted us to examine their respective emission behavior (see SI, Section S9) by solid-state photoluminescence spectroscopy in the presence of different small molecule analytes to determine their potential for sensing. Emission spectra were collected for dry and wetted ligands, diesters and-MOFs, as well as MOF samples in the presence of gaseous N_2, CO_2 and H_2S. Small shifts in emission maxima were observed when the MOFs were exposed to various gases, although the most significant changes occurred upon wetting (see SI, Figure S27), which was not evident for the diesters (see SI, Figure S26). For example, **Zr-L1** shows a demonstrable red-shift upon exposure to a hydrated environment, with λ_{em} = 407 nm drifting to 423 nm, and Φ_F decreasing from 0.17 to 0.12 (Figure 6a).

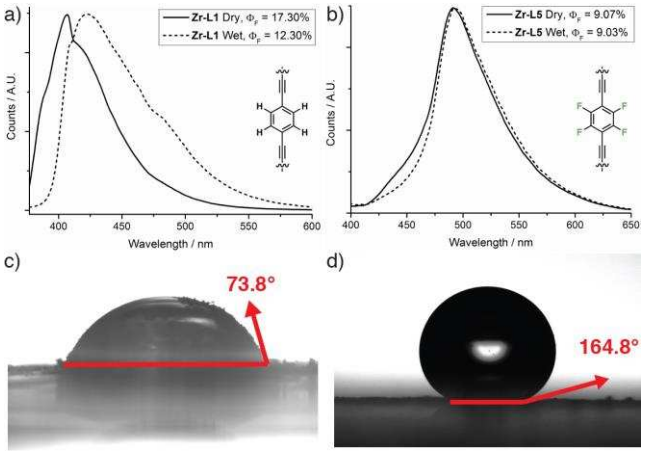

Figure 6. Normalized solid-state photoluminescence emission profiles of a) **Zr-L1** and b) **Zr-L5**, under dry and wet conditions. Contact angles were measured for c) **Zr-L1** and d) **Zr-L5**.

We see no such effects with **Zr-L5**, where the central aryl-moiety of **L5** is decorated with four fluorine atoms. The emission profiles are almost identical under both dry and wet conditions with little impact upon Φ_F (Figure 6b). Having pores lined with fluorine atoms, we posit that the fluorescence emission of **Zr-L5** does not change under hydrating conditions due to the increased hydrophobicity of the material, preventing water from penetrating into and interacting with the framework. Contact angles of packed powdered samples of **Zr-L1** and **Zr-L5** were measured to understand whether differences in hydrophobicity are responsible for the different emission behaviors (Figure 6c, 6d, and SI Section 10). **Zr-L1** has a contact angle of ~73.8° indicative of a hydrophilic material, while **Zr-L5** has a contact angle of ~164.8° which is typical of superhydrophobic materials.[70]

These measurements show that small changes to the bridging organic ligand can considerably alter the MOFs hydrophobicity.[71] Recently, during a report by Maji *et al.*, a self-cleaning Zn MOF containing alkoxyoctadecyl (C_{18}) substituted peb^{2-} ligands displayed superhydrophobic behaviour,[72] while MOFs containing fluorine-abundant ligands have been shown to be hydrophobic.[73,74] In contrast, we have shown that, by substitution of only one third of the aromatic protons for fluorine atoms in the organic ligand, one can generate a superhydrophobic surface comparable to the remarkable examples detailed above.[70-74] **Zr-L5** is an example of a stable, carboxylate-based fluorinated MOF, and we anticipate that other functionalized peb^{2-} ligands could be synthesized and incorporated into interpenetrated Zr MOFs to control hydrophobicity.

Of all the MOFs examined, **Zr-L6** and **Zr-L7** exhibited the most significant changes in the presence of the different analytes likely as a consequence of the intrinsic fluorescence of their functional units. The solid-state fluorescence emission of evacuated **Zr-L7** (λ_{em} = 500 nm; λ_{ex} = 468 nm, Figure 7) is noticeably different to the corresponding diester **L7-Me$_2$** (λ_{em} = 525 nm; λ_{ex} = 450 nm),

with a hypsochromic shift in the major emission band due to separation of ligands in the MOF removing any inter-ligand CT, as well as the influence of the more accessible LCCT noted above. More specifically, **Zr-L7** exhibits two clear transitions centered at 500 nm and 525 nm. For both MOFs, the most sensitive fluorescence emission change is observed upon hydration, with the pronounced changes in **Zr-L7** suggesting application as a water vapor sensor (Figure 7).

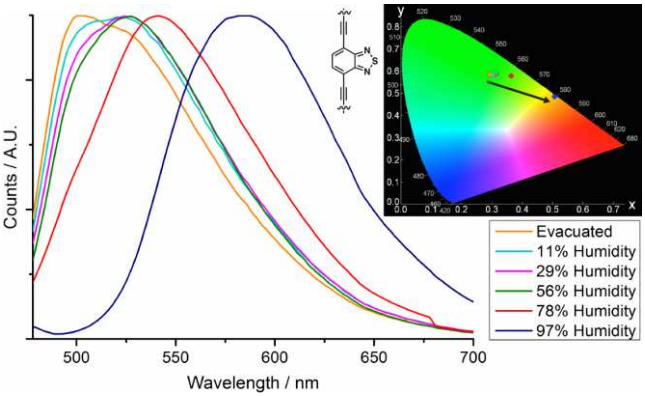

Figure 7. Normalized solid-state photoluminescence spectra of **Zr-L7** upon exposure to differing relative humidity (λ_{ex} = 468 nm). Inset: Chromaticity diagram demonstrating dramatic red-shift at 97% humidity.

As **Zr-L7** is exposed to hydrated environments, the 500 nm emission band begins to quench while the emission at 525 nm redshifts to 586 nm (both at 97% relative humidity (H_{rel}) and when wetted, λ_{ex} = 468 nm); a significant λ_{max} color shift of 86 nm (see chromaticity in Figure 7 inset). **Zr-L7** also exhibits the largest response factor (RF = $(\lambda_{max}/\lambda_o)$-1 where λ_o is the emission of dried **Zr-L7**) for H_{rel} = 97% for a Zr-MOF at 0.17.[75] Particularly noteworthy is the emission shift at H_{rel} levels as low as 11% (RF = 0.05) demonstrating the high sensitivity of this material towards water vapor. Of the other MOFs, **Zr-L6** shows the most significant changes in emission as humidity increases with a bathochromic shift of λ_{em} from 487 nm to 521 nm (see SI, Figure S36), while gaseous CO_2, N_2 and H_2S cause slight alterations to the fluorescence emission of both **Zr-L6** and **Zr-L7** (see SI, Figure S34).

We believe that hydration of the nodes,[76] coupled with the degree of conjugation for **Zr-L7** (and **Zr-L6**) results in the raising of the HOMO levels for the noted LCCT, causing a slight bathochromic shift in the solid-state absorption spectrum (see SI, Figure S38) and dramatic red-shift in the emission. For **Zr-L7** this is further shifted by cooperative hydrogen bonding effects with **L7** (as seen with other protic solvents), compared with **Zr-L6** where hydrogen bonding to the naphthyl units is not possible. Few studies have reported intrinsic fluorescence sensing of water by MOFs.[75,77-79] This is noteworthy since Zr-MOFs are ideal platforms for water sorption[32] and sensing applications due to their well-known aqueous stability,[45,80,81] and inherent vacancies made available upon activation from indiscriminately defective Zr-clusters within the networks.[28,82,83] Indeed, PXRD analysis shows **Zr-L7** was unchanged after the humidity profile was collected (see SI, Figure S39).

In parallel to the emission studies noted above, we examined the photoluminescence spectra of the MOFs in the presence of liquid analytes, with a range of different behaviors observed across the series (see SI, Figure S40). **Zr-L2** exhibits the most pronounced solvatochromism of the series, with a modest trend relating to solvent dipole moment (Figure 8; where interacting water (node coordination) and toluene (π-stacking) behave as outliers). In contrast, **Zr-L7** demonstrates less pronounced solvatochromism, with no distinct trends relating to solvent dipole moment, dielectric, or polarity indices.

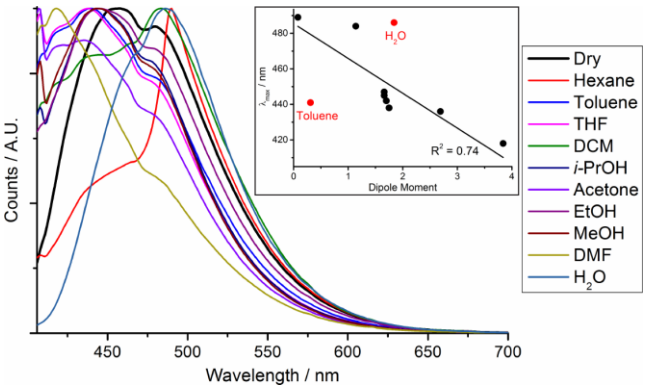

Figure 8. Normalized solid-state photoluminescence emission spectra of **Zr-L2** after exposure to various solvents (λ_{ex} = 396 nm). Inset: Correlation of change in λ_{max} with solvent dipole moment; water and toluene have been excluded from correlation as they demonstrate direct interaction.

It is worth noting that **L2-Me$_2$** and **L7-Me$_2$** show no distinctive solvent dependent emission shifts in the solid-state (see SI, Figure S43), in contrast to their respective Zr MOFs. This confirms the requirement of the framework topology for the solvent and hydration dependent emission behavior.

Interestingly, **Zr-L2** exhibits two radiative transitions in its emission profile (Figure 9), which appear to be inherited from the ligand (see SI, Section 9). We hypothesize that the two radiative transitions are related to differing ligand conformations derived from twisting of the central dimethylphenylene units, as seen in its solid-state structure; twisting of the bridging dimethyphenylene moiety is also present in the crystal structure of **L2-Me$_2$** (see SI, Figure S3). In comparison with the emission spectrum of dried **Zr-L2**, the intensity of the transition at 465 nm decreases upon wetting. This decrease in intensity suggests that water is causing a structural perturbation of the MOF, presumably by altering the degree of ligand twisting. Furthermore, the decrease in intensity at λ_{em} = 465 nm is accompanied with an increase in Φ_F, indicative of a higher population of decay centered on the transition at λ_{em} = 486 nm. It is worth noting that this observation is purely with material that has been exposed to liquid water; exposure to a range of increasing H_{rel} values perturbs the system only minimally. Coupled with the observed crystallographic transformation from the orthorhombic

(twisted/planar ligands) to cubic structure (planar ligands) under heating noted above, these emission data lead us to believe that wetting may result in an increased population of the planar ligand conformation.

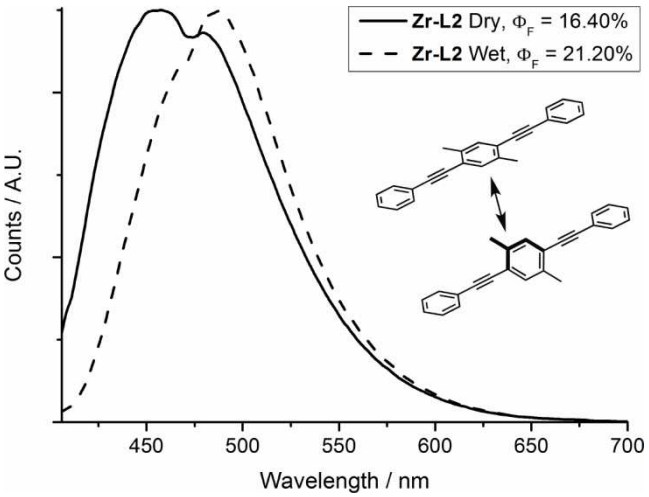

Figure 9. Normalized solid-state photoluminescence emission of **Zr-L2** under dry and wet conditions alongside a schematic representation of the observed twisting of the ligands (λ_{ex} = 396 nm).

From these results, it is clear that solid-state photoluminescence spectroscopy is a versatile tool to not only probe host-guest interactions in MOFs (with potential for sensing) but also physical properties such as hydrophobicity, and subtle structural features such as the ligand rotation phenomenon observed in **Zr-L2**.

Conclusions

We have prepared a series of interpenetrated Zr and Hf MOFs comprised of functionalized 4,4′-[1,4-phenylene-bis(ethyne-2,1-diyl)]-dibenzoate ligands, and shown that while functionalization does not affect overall topology, it does induce subtle changes in linker orientation and net-net interactions in the solid-state. In particular, the pendant methyl groups of **Zr-L2** induce a change in crystal habit and symmetry, through steric clashes and resultant twisting of dimethylphenylene units to form an orthorhombic structure, which can subsequently be converted to the parent cubic form by heating, with the twisted dimethylphenylene units returning to planarity. The MOFs have excellent porosity, with the introduction of aromatic units and nucleophilic heterocycles enhancing CO_2 uptake. Access to this related series of MOFs with intrinsically fluorescent linkers has allowed us to probe their structures and properties using solid-state photoluminescence spectroscopy, demonstrating the versatility and potential power of the technique. The subtle structural changes described for **Zr-L2** can be observed in the relative intensities of different emission maxima when spectra are collected under different conditions. Incorporation of naphthyl and benzothiadiazolyl fluorophores, into **Zr-L6** and **Zr-L7** respectively, generates MOFs that can detect guest molecules, with highly sensitive emission changes upon wetting and structural stability suggesting possible use of **Zr-L7** as a water sensor. Additionally, the superhydrophobicity of the partially fluorinated **Zr-L5** can be seen by the close correlation between its spectra collected when wet and dry, in contrast to the large shifts seen for the hydrophilic **Zr-L1**, and these results have been confirmed by contact angle measurements.

The fact that functionalization of the peb^{2-} scaffold induces such structural and physical variety in the resulting MOFs, coupled with the fact that many of the properties are not present in the free ligands, has allowed us to demonstrate not only the potential of the series for simple introduction of versatile functionality into MOFs to enhance their physical properties, but also the potential for using photoluminescence spectroscopy as a facile technique to probe these subtle changes in MOF structure, physical properties and host-guest interactions. We also expect the dynamic behavior of these interpenetrated Zr and Hf MOFs to modulate their mechanical properties, while studies investigating modulation of their physical and optical properties by synthesizing new functionalized analogues are underway.

ASSOCIATED CONTENT

Supporting Information. Synthesis of all ligands and MOFs, PXRD, TGA, gas adsorption analysis, solid-state UV-Vis and photoluminescence spectroscopy. This material is available free of charge via the Internet at http://pubs.acs.org. The data which underpin this work are available at http://dx.doi.org/10.5525/gla.researchdata.398. CCDC 1516193-1516211 contain the supplementary crystallographic data for this paper.

AUTHOR INFORMATION

Corresponding Author

*Ross.Forgan@glasgow.ac.uk; *B.Blight@unb.ca

Author Contributions

All authors have given approval to the final version of the manuscript.

ACKNOWLEDGMENT

RSF thanks the Royal Society for receipt of a University Research Fellowship and the University of Glasgow for funding. The research was supported by EPSRC (EP/L004461/1). BAB thanks the University of Kent for funding and Edinburgh Instruments (Livingston, UK) for in-kind support. YK is a DSTL-funded post-graduate researcher. We thank Mauro Davide Cappelluti and Prof Duncan Gregory for access to solid-state UV-Vis facilities, Rigaku OD for single crystal data collection of **Zr-L2** and the EPSRC UK National Crystallographic Service for single crystal data collection.[84]

REFERENCES

(1) Hoskins, B. F.; Robson, R. *J. Am. Chem. Soc.* **1990**, *112*, 1546.
(2) Kondo, M.; Yoshitomi, T.; Matsuzaka, H.; Kitagawa, S.; Seki, K. *Angew. Chem., Int. Ed. Engl.* **1997**, *36*, 1725.
(3) Chui, S. S.-Y.; Lo, S. M.-F.; Charmant, J. P. H.; Orpen, A. G.; Williams, I. D. *Science* **1999**, *283*, 1148.

(4) Li, H.; Eddaoudi, M.; O'Keeffe, M.; Yaghi, O. M. *Nature* **1999**, *402*, 276.
(5) Seo, J. S.; Whang, D.; Lee, H.; Jun, S. I.; Oh, J.; Jeon, Y. J.; Kim, K. *Nature* **2000**, *404*, 982.
(6) Long, J. R.; Yaghi, O. M. *Chem. Soc. Rev.* **2009**, *38*, 1213.
(7) Zhou, H.-C.; Long, J. R.; Yaghi, O. M. *Chem. Rev.* **2012**, *112*, 673.
(8) Yaghi, O. M.; O'Keeffe, M.; Ockwig, N. W.; Chae, H. K.; Eddaoudi, M.; Kim, J. *Nature* **2003**, *423*, 705.
(9) Kitagawa, S.; Kitaura, R.; Noro, S.-i. *Angew. Chem. Int. Ed.* **2004**, *43*, 2334.
(10) Lu, W.; Wei, Z.; Gu, Z.-Y.; Liu, T.-F.; Park, J.; Park, J.; Tian, J.; Zhang, M.; Zhang, Q.; Gentle Iii, T.; Bosch, M.; Zhou, H.-C. *Chem. Soc. Rev.* **2014**, *43*, 5561.
(11) He, Y.; Zhou, W.; Qian, G.; Chen, B. *Chem. Soc. Rev.* **2014**, *43*, 5657.
(12) Murray, L. J.; Dinca, M.; Long, J. R. *Chem. Soc. Rev.* **2009**, *38*, 1294.
(13) Tranchemontagne, D. J.; Park, K. S.; Furukawa, H.; Eckert, J.; Knobler, C. B.; Yaghi, O. M. *J. Phys. Chem. C.* **2012**, *116*, 13143.
(14) Li, J.-R.; Kuppler, R. J.; Zhou, H.-C. *Chem. Soc. Rev.* **2009**, *38*, 1477.
(15) Sumida, K.; Rogow, D. L.; Mason, J. A.; McDonald, T. M.; Bloch, E. D.; Herm, Z. R.; Bae, T.-H.; Long, J. R. *Chem. Rev.* **2012**, *112*, 724.
(16) Zhang, Z.; Zhao, Y.; Gong, Q.; Li, Z.; Li, J. *Chem. Commun.* **2013**, *49*, 653.
(17) Lee, J.; Farha, O. K.; Roberts, J.; Scheidt, K. A.; Nguyen, S. T.; Hupp, J. T. *Chem. Soc. Rev.* **2009**, *38*, 1450.
(18) Yoon, M.; Srirambalaji, R.; Kim, K. *Chem. Rev.* **2012**, *112*, 1196.
(19) Liu, J.; Chen, L.; Cui, H.; Zhang, J.; Zhang, L.; Su, C.-Y. *Chem. Soc. Rev.* **2014**, *43*, 6011.
(20) Cui, Y.; Yue, Y.; Qian, G.; Chen, B. *Chem. Rev.* **2012**, *112*, 1126.
(21) Kreno, L. E.; Leong, K.; Farha, O. K.; Allendorf, M.; Van Duyne, R. P.; Hupp, J. T. *Chem. Rev.* **2012**, *112*, 1105.
(22) Hu, Z.; Deibert, B. J.; Li, J. *Chem. Soc. Rev.* **2014**, *43*, 5815.
(23) Horcajada, P.; Serre, C.; Vallet-Regí, M.; Sebban, M.; Taulelle, F.; Férey, G. *Angew. Chem. Int. Ed.* **2006**, *45*, 5974.
(24) McKinlay, A. C.; Morris, R. E.; Horcajada, P.; Férey, G.; Gref, R.; Couvreur, P.; Serre, C. *Angew. Chem. Int. Ed.* **2010**, *49*, 6260.
(25) Della Rocca, J.; Liu, D.; Lin, W. *Acc. Chem. Res.* **2011**, *44*, 957.
(26) Orellana-Tavra, C.; Baxter, E. F.; Tian, T.; Bennett, T. D.; Slater, N. K. H.; Cheetham, A. K.; Fairen-Jimenez, D. *Chem. Commun.* **2015**, *51*, 13878.
(27) Cavka, J. H.; Jakobsen, S.; Olsbye, U.; Guillou, N.; Lamberti, C.; Bordiga, S.; Lillerud, K. P. *J. Am. Chem. Soc.* **2008**, *130*, 13850.
(28) Cliffe, M. J.; Wan, W.; Zou, X.; Chater, P. A.; Kleppe, A. K.; Tucker, M. G.; Wilhelm, H.; Funnell, N. P.; Coudert, F.-X.; Goodwin, A. L. *Nat Commun* **2014**, *5*.
(29) Feng, D.; Jiang, H.-L.; Chen, Y.-P.; Gu, Z.-Y.; Wei, Z.; Zhou, H.-C. *Inorg. Chem.* **2013**, *52*, 12661.
(30) Valenzano, L.; Civalleri, B.; Chavan, S.; Bordiga, S.; Nilsen, M. H.; Jakobsen, S.; Lillerud, K. P.; Lamberti, C. *Chem. Mater.* **2011**, *23*, 1700.
(31) Bai, Y.; Dou, Y.; Xie, L.-H.; Rutledge, W.; Li, J.-R.; Zhou, H.-C. *Chem. Soc. Rev.* **2016**, *45*, 2327.
(32) Furukawa, H.; Gándara, F.; Zhang, Y.-B.; Jiang, J.; Queen, W. L.; Hudson, M. R.; Yaghi, O. M. *J. Am. Chem. Soc.* **2014**, *136*, 4369.
(33) Ma, J.; Wong-Foy, A. G.; Matzger, A. J. *Inorg. Chem.* **2015**, *54*, 4591.
(34) Wang, R.; Wang, Z.; Xu, Y.; Dai, F.; Zhang, L.; Sun, D. *Inorg. Chem.* **2014**, *53*, 7086.
(35) Feng, D.; Gu, Z.-Y.; Li, J.-R.; Jiang, H.-L.; Wei, Z.; Zhou, H.-C. *Angew. Chem. Int. Ed.* **2012**, *51*, 10307.
(36) Morris, W.; Volosskiy, B.; Demir, S.; Gándara, F.; McGrier, P. L.; Furukawa, H.; Cascio, D.; Stoddart, J. F.; Yaghi, O. M. *Inorg. Chem.* **2012**, *51*, 6443.
(37) Mondloch, J. E.; Bury, W.; Fairen-Jimenez, D.; Kwon, S.; DeMarco, E. J.; Weston, M. H.; Sarjeant, A. A.; Nguyen, S. T.; Stair, P. C.; Snurr, R. Q.; Farha, O. K.; Hupp, J. T. *J. Am. Chem. Soc.* **2013**, *135*, 10294.
(38) Schaate, A.; Roy, P.; Preuße, T.; Lohmeier, S. J.; Godt, A.; Behrens, P. *Chem. Eur. J.* **2011**, *17*, 9320.
(39) Lippke, J.; Brosent, B.; von Zons, T.; Virmani, E.; Lilienthal, S.; Preuße, T.; Hülsmann, M.; Schneider, A. M.; Wuttke, S.; Behrens, P.; Godt, A. *Inorg. Chem.*, **2017**, *56*, 748.
(40) Chen, D.; Xing, H.; Wang, C.; Su, Z. *J. Mater. Chem. A* **2016**, *4*, 2657.
(41) Doan, T. L. H.; Nguyen, H. L.; Pham, H. Q.; Pham-Tran, N.-N.; Le, T. N.; Cordova, K. E. *Chem. Asian J.* **2015**, *10*, 2660.
(42) Doan, T. L. H.; Dao, T. Q.; Tran, H. N.; Tran, P. H.; Le, T. N. *Dalton Trans.* **2016**, *45*, 7875.
(43) Babarao, R.; Rubio-Martinez, M.; Hill, M. R.; Thornton, A. W. *J. Phys. Chem. C.* **2016**, *120*, 13013.
(44) Marshall, R. J.; Griffin, S. L.; Wilson, C.; Forgan, R. S. *J. Am. Chem. Soc.* **2015**, *137*, 9527.
(45) Marshall, R. J.; Griffin, S. L.; Wilson, C.; Forgan, R. S. *Chem. Eur. J.* **2016**, *22*, 4870.
(46) Hobday, C. L.; Marshall, R. J.; Murphie, C. F.; Sotelo, J.; Richards, T.; Allan, D. R.; Düren, T.; Coudert, F.-X.; Forgan, R. S.; Morrison, C. A.; Moggach, S. A.; Bennett, T. D. *Angew. Chem. Int. Ed.* **2016**, *55*, 2401.
(47) Marshall, R. J.; Richards, T.; Hobday, C. L.; Murphie, C. F.; Wilson, C.; Moggach, S. A.; Bennett, T. D.; Forgan, R. S. *Dalton Trans.* **2016**, *45*, 4132.
(48) Fasina, T. M.; Collings, J. C.; Burke, J. M.; Batsanov, A. S.; Ward, R. M.; Albesa-Jove, D.; Porres, L.; Beeby, A.; Howard, J. A. K.; Scott, A. J.; Clegg, W.; Watt, S. W.; Viney, C.; Marder, T. B. *J. Mater. Chem.* **2005**, *15*, 690.
(49) Carboni, M.; Lin, Z.; Abney, C. W.; Zhang, T.; Lin, W. *Chem. Eur. J.* **2014**, *20*, 14965.
(50) Nagarkar, S. S.; Desai, A. V.; Ghosh, S. K. *Chem. Commun.* **2014**, *50*, 8915.
(51) Nagarkar, S. S.; Desai, A. V.; Ghosh, S. K. *Chem. Eur. J.* **2015**, *21*, 9994.
(52) Desai, A. V.; Samanta, P.; Manna, B.; Ghosh, S. K. *Chem. Commun.* **2015**, *51*, 6111.
(53) Drache, F.; Bon, V.; Senkovska, I.; Adam, M.; Eychmüller, A.; Kaskel, S. *Eur. J. Inorg. Chem.* **2016**, 4483.
(54) Wang, B.; Lv, X.-L.; Feng, D.; Xie, L.-H.; Zhang, J.; Li, M.; Xie, Y.; Li, J.-R.; Zhou, H.-C. *J. Am. Chem. Soc.* **2016**, *138*, 6204.
(55) Jiang, H.-L.; Feng, D.; Wang, K.; Gu, Z.-Y.; Wei, Z.; Chen, Y.-P.; Zhou, H.-C. *J. Am. Chem. Soc.* **2013**, *135*, 13934.
(56) Aguilera-Sigalat, J.; Bradshaw, D. *Chem. Commun.* **2014**, *50*, 4711.
(57) Wei, Z.; Gu, Z.-Y.; Arvapally, R. K.; Chen, Y.-P.; McDougald, R. N.; Ivy, J. F.; Yakovenko, A. A.; Feng, D.; Omary, M. A.; Zhou, H.-C. *J. Am. Chem. Soc.* **2014**, *136*, 8269.
(58) Deria, P.; Yu, J.; Balaraman, R. P.; Mashni, J.; White, S. *Chem. Commun.* **2016**, *52*, 13031.
(59) Roy, P.; Schaate, A.; Behrens, P.; Godt, A. *Chem. Eur. J.* **2012**, *18*, 6979.

(60) Marshall, R. J.; Hobday, C. L.; Murphie, C. F.; Griffin, S. L.; Morrison, C. A.; Moggach, S. A.; Forgan, R. S. *J. Mater. Chem. A* **2016**, *4*, 6955.
(61) Gutov, O. V.; Molina, S.; Escudero-Adán, E. C.; Shafir, A. *Chem. Eur. J.* **2016**, *22*, 13582.
(62) Song, C.; He, Y.; Li, B.; Ling, Y.; Wang, H.; Feng, Y.; Krishna, R.; Chen, B. *Chem. Commun.* **2014**, *50*, 12105.
(63) Gutierrez Tovar, M.; Cohen, B.; Sanchez, F.; Douhal, A. *Phys. Chem. Chem. Phys.* **2016**, *18*, 27761.
(64) Mallick, A.; Garai, B.; Addicoat, M. A.; Petkov, P. S.; Heine, T.; Banerjee, R. *Chem. Sci.* **2015**, *6*, 1420.
(65) Parker, T. C.; Patel, D. G.; Moudgil, K.; Barlow, S.; Risko, C.; Bredas, J.-L.; Reynolds, J. R.; Marder, S. R. *Mater. Horiz.* **2015**, *2*, 22.
(66) Neto, B. A. D.; Carvalho, P. H. P. R.; Correa, J. R. *Acc. Chem. Res.* **2015**, *48*, 1560.
(67) Pritchard, V. E.; Thorp-Greenwood, F. L.; Balasingham, R. G. Williams, C. F.; Kariuki, B. M.; Platts, J. A.; Hallet, A. J.; Coogan, M. P. *Organometallics*, **2013**, *32*, 3566.
(68) Fu, Y.; Sun, D.; Chen, Y.;Huang, R.; Ding, Z.; Fu, X.; Li, Z. *Angew. Chem. Int. Ed.* **2012**, *51*, 3364.
(69) Horiuchi, Y.; Toyao, T.; Saito, M.; Mochizuki, K.; Iwata, M.; Higashimura, H.; Anpo, M.; Matsuoku, M. *J. Phys. Chem. C.* **2012**, *116*, 20848.
(70) Law, K.-Y. *J. Phys. Chem. Lett.* **2014**, *5*, 686.
(71) Nguyen, J. G.; Cohen, S. M. *J. Am. Chem. Soc.* **2010**, *132*, 4560.
(72) Roy, S.; Suresh, V. M.; Maji, T. K. *Chem. Sci.* **2016**, *7*, 2251.
(73) Chen, T.-H.; Popov, I.; Zenasni, O.; Daugulis, O.; Miljanic, O. S. *Chem. Commun.* **2013**, *49*, 6846.
(74) Chen, T.-H.; Popov, I.; Kaveevivitchai, W.; Chuang, Y.-C.; Chen, Y.-S.; Jacobson, A. J.; Miljanić, O. Š. *Angew. Chem. Int. Ed.* **2015**, *54*, 13902.
(75) Drache, F.; Bon, V.; Senkovska, I.; Adam, M.; Eychmüller, A.; Kaskel, S. *Eur. J. Inorg. Chem.* **2016**, *2016*, 4483.
(76) The hydrogen bonding of water to μ_3-OH units of $Zr_6O_4(OH)_4$ clusters in related Zr MOFs has been observed crystallographically. See: Ko, N.; Hong, J.; Sung, S.; Cordova, K. E.; Park, H. J.; Yang, J. K.; Kim, J. *Dalton Trans.*, **2015**, *44*, 2047.
(77) Yu, Y.; Zhang, X.-M.; Ma, J.-P.; Liu, Q.-K.; Wang, P.; Dong, Y.-B. *Chem. Commun.* **2014**, *50*, 1444.
(78) Douvali, A.; Tsipis, A. C.; Eliseeva, S. V.; Petoud, S.; Papaefstathiou, G. S.; Malliakas, C. D.; Papadas, I.; Armatas, G. S.; Margiolaki, I.; Kanatzidis, M. G.; Lazarides, T.; Manos, M. J. *Angew. Chem. Int. Ed.* **2015**, *54*, 1651.
(79) Fard, Z. H.; Kalinovskyy, Y.; Spasyuk, D. M.; Blight, B. A.; Shimizu, G. K. H. *Chem. Commun.* **2016**, *52*, 12865.
(80) Liu, X.; Demir, N. K.; Wu, Z.; Li, K. *J. Am. Chem. Soc.* **2015**, *137*, 6999.
(81) Mondloch, J. E.; Katz, M. J.; Planas, N.; Semrouni, D.; Gagliardi, L.; Hupp, J. T.; Farha, O. K. *Chem. Commun.* **2014**, *50*, 8944.
(82) Katz, M. J.; Brown, Z. J.; Colon, Y. J.; Siu, P. W.; Scheidt, K. A.; Snurr, R. Q.; Hupp, J. T.; Farha, O. K. *Chem. Commun.* **2013**, *49*, 9449.
(83) Shearer, G. C.; Chavan, S.; Ethiraj, J.; Vitillo, J. G.; Svelle, S.; Olsbye, U.; Lamberti, C.; Bordiga, S.; Lillerud, K. P. *Chem. Mater.* **2014**, *26*, 4068.
(84) Coles, S. J.; Gale, P. A. *Chem. Sci.* **2012**, *3*, 683.

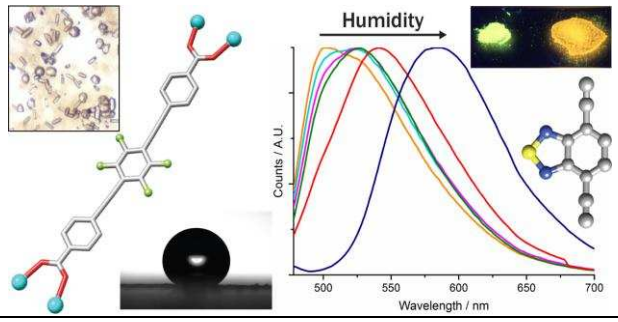
Humidity
Counts / A.U.
500
550
600
650
700
Wavelength / nm

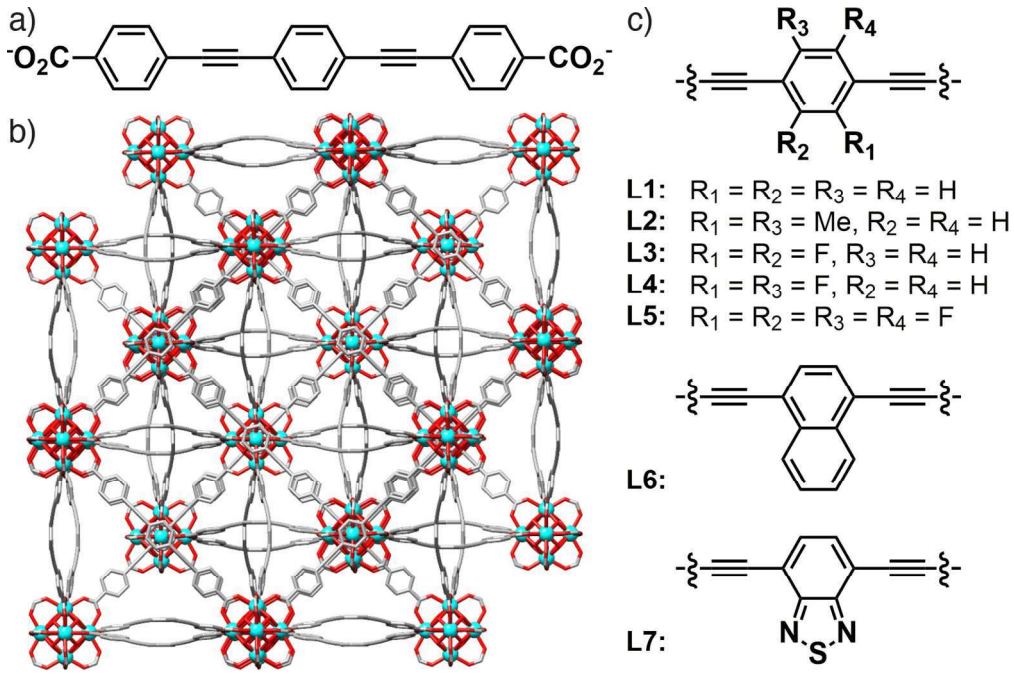

Figure 1 - single column

142x94mm (300 x 300 DPI)

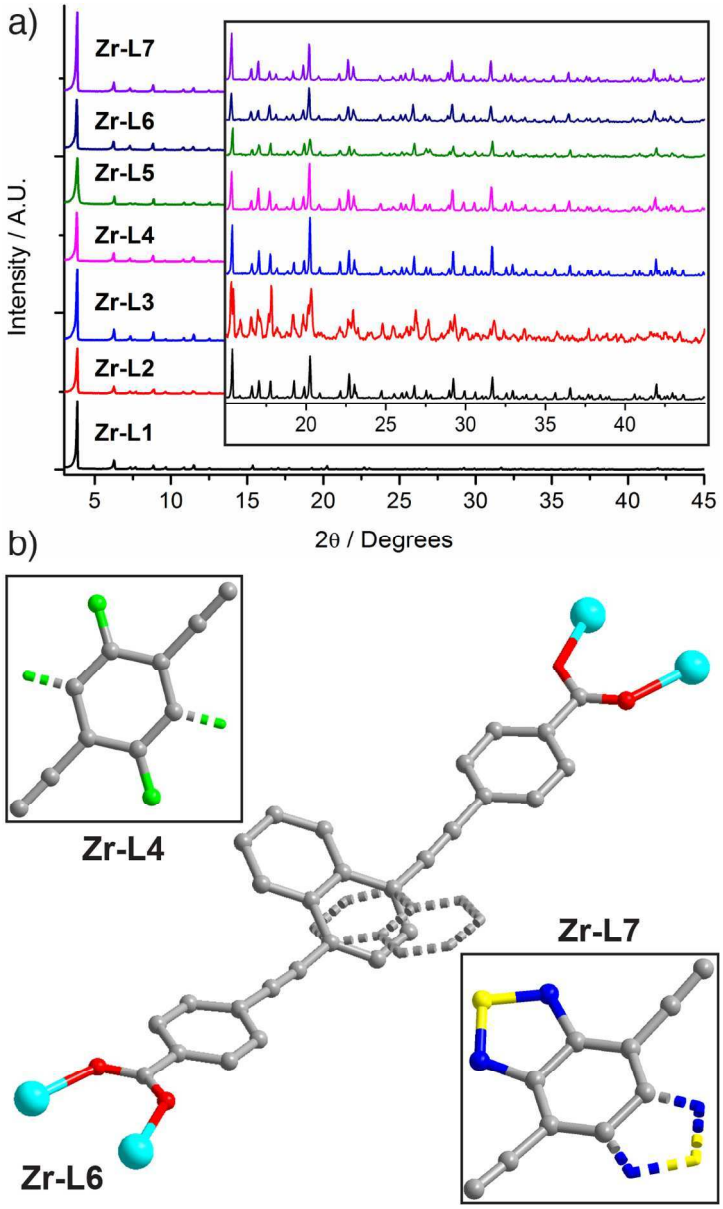

Figure 2 - single column

99x166mm (300 x 300 DPI)

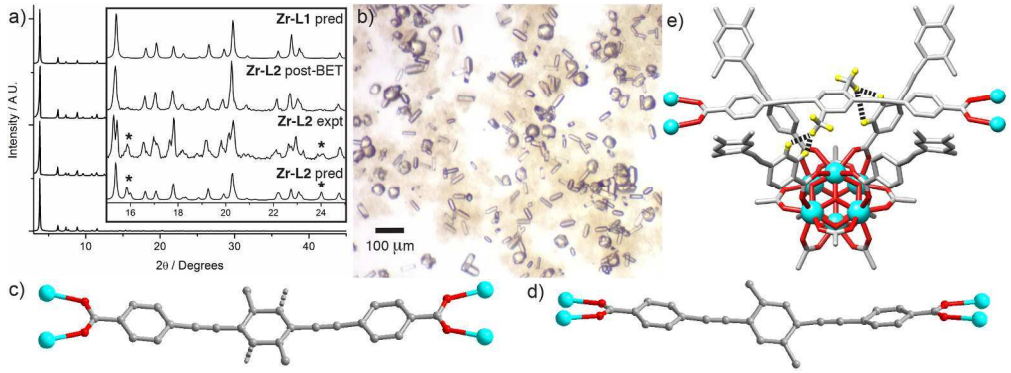

Figure 3 - double column

199x73mm (300 x 300 DPI)

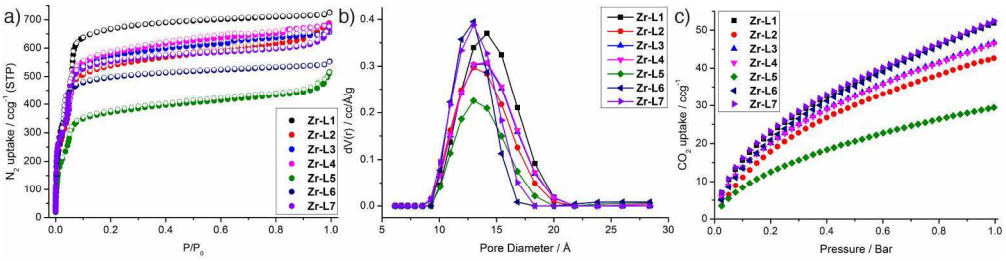

d)

	L1	L2	L3	L4	L5	L6	L7
Zr	2680 m^2g^{-1}	2070 m^2g^{-1}	2195 m^2g^{-1}	2270 m^2g^{-1}	1420 m^2g^{-1}	1990 m^2g^{-1}	2130 m^2g^{-1}
Hf	2080 m^2g^{-1}	1775 m^2g^{-1}	1800 m^2g^{-1}	1960 m^2g^{-1}	675 m^2g^{-1}	1210 m^2g^{-1}	1660 m^2g^{-1}

Figure 4 - double column

197x71mm (300 x 300 DPI)

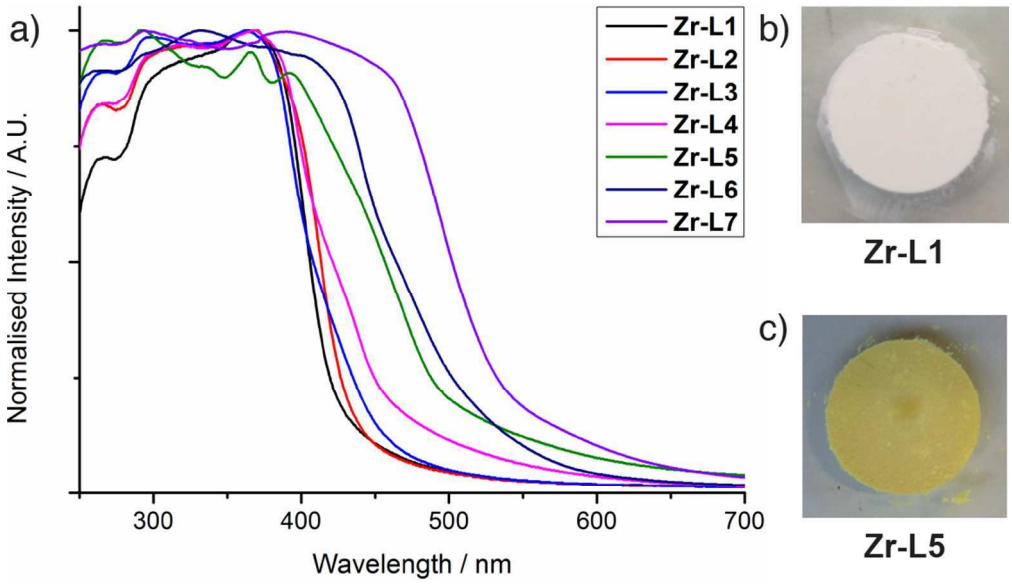

Figure 5 - single column

97x56mm (300 x 300 DPI)

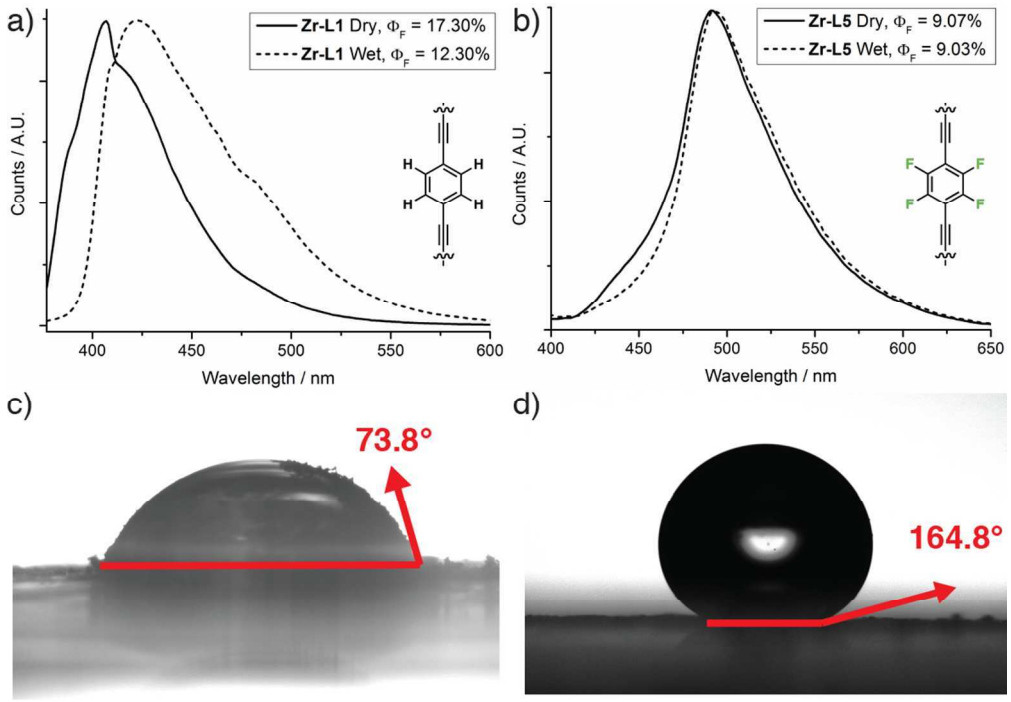

Figure 6 - single column

99x69mm (300 x 300 DPI)

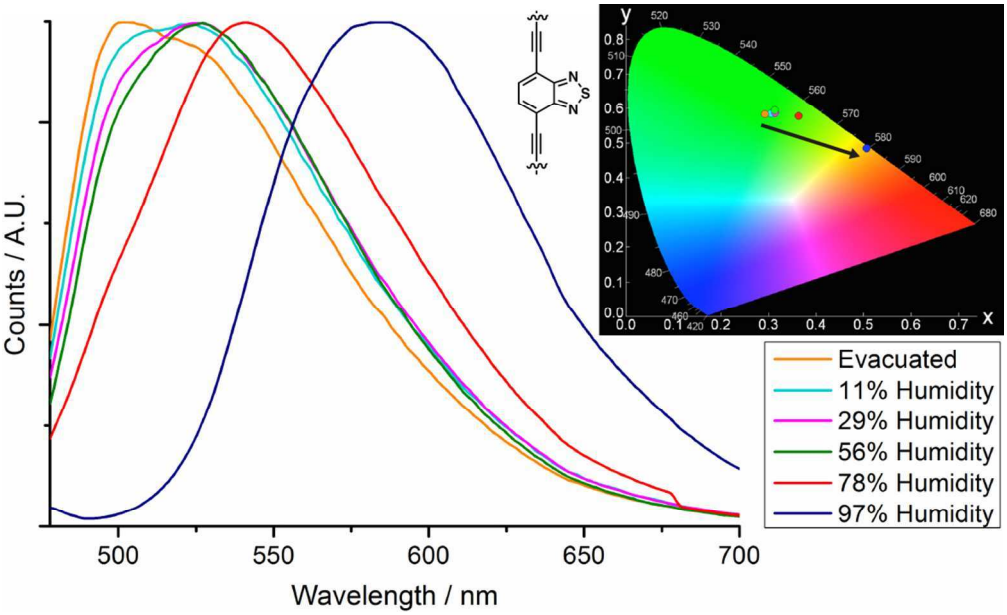

Figure 7 - single column

99x60mm (300 x 300 DPI)

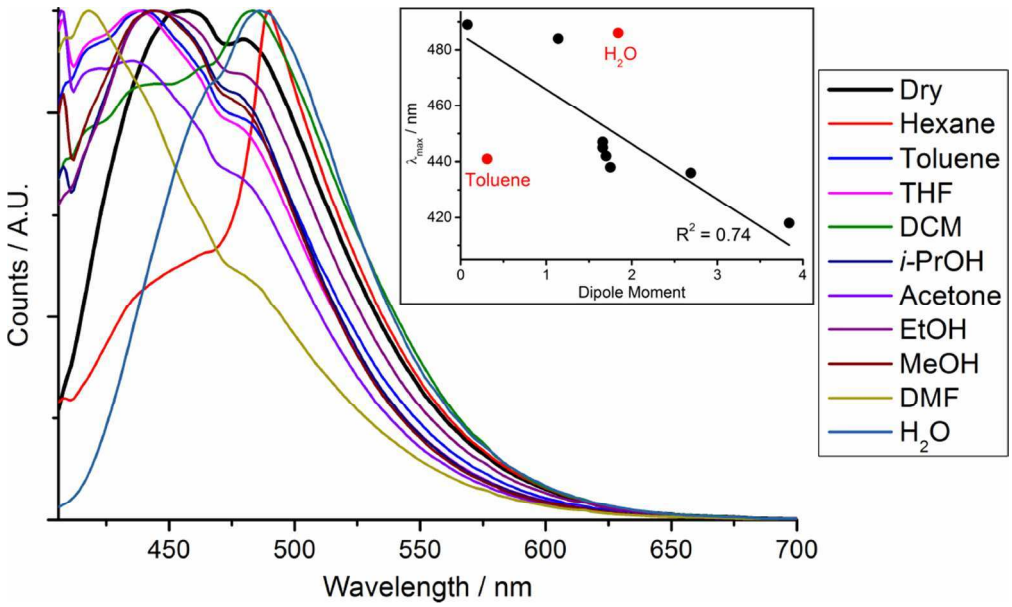

Figure 8 - single column

98x58mm (300 x 300 DPI)

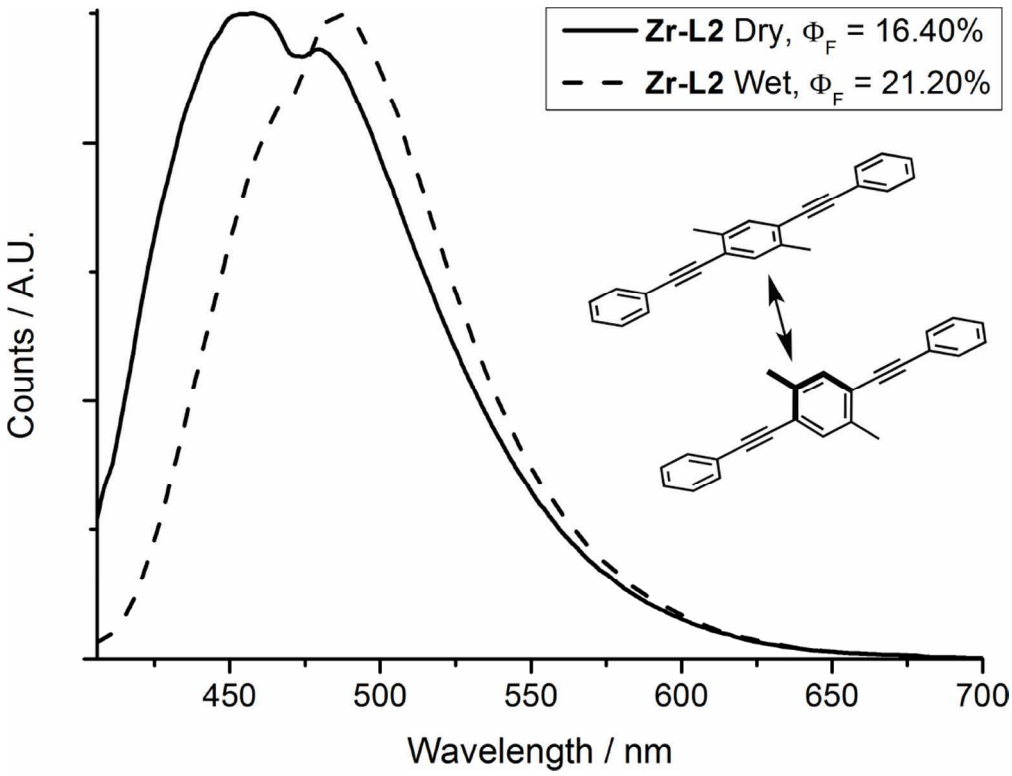

Figure 9 - single column

98x74mm (300 x 300 DPI)

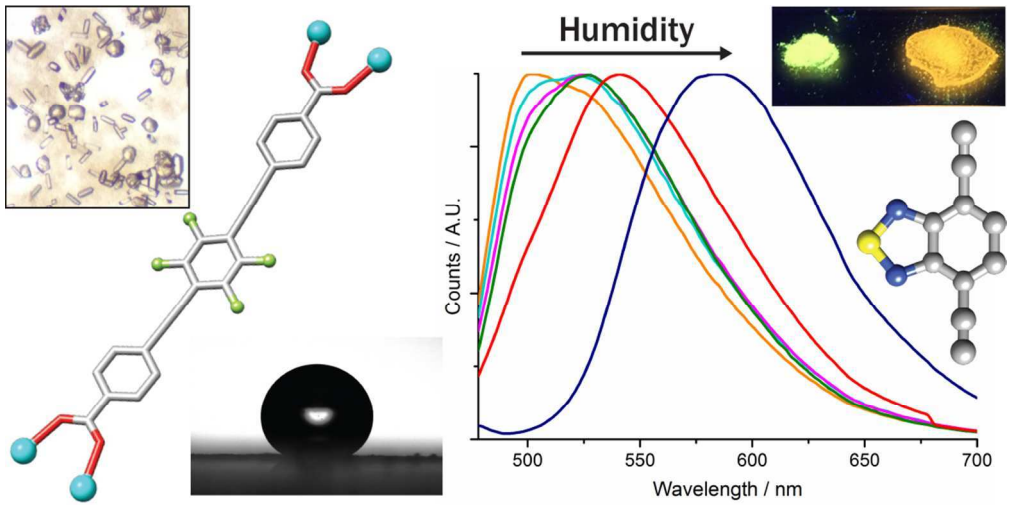

TOC image

99x49mm (300 x 300 DPI)